Volume 20 | Number 44 | 28 November 2018 | Pages 7033–7222

CrystEngComm

rsc.li/crystengcomm

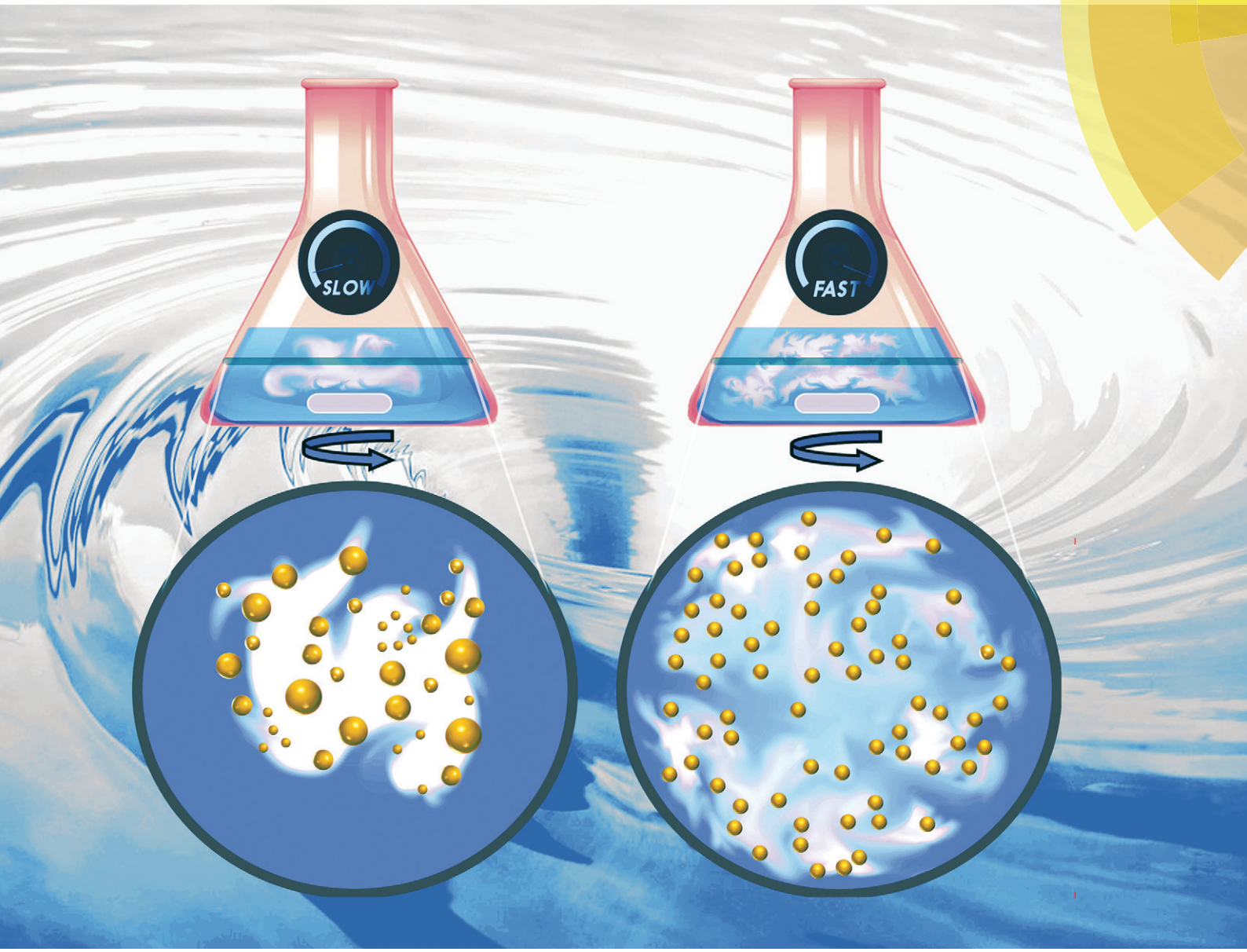

ROYAL SOCIETY OF CHEMISTRY

PAPER

Maximilian O. Besenhard, Nguyen T. K. Thanh, Asterios Gavriilidis *et al.*
New insight into the effect of mass transfer on the synthesis of silver and gold nanoparticles

CrystEngComm

PAPER

View Article Online
View Journal | View Issue

Cite this: *CrystEngComm*, 2018, **20**, 7082

New insight into the effect of mass transfer on the synthesis of silver and gold nanoparticles†

Maximilian O. Besenhard, [a] Razwan Baber,[a] Alec P. LaGrow, [b] Luca Mazzei, [a] Nguyen T. K. Thanh *[bc] and Asterios Gavriilidis *[a]

The fact that mass transfer affects noble metal nanoparticle (NP) syntheses is well known, not least because the scale-up of batch processes is anything but trivial. Therefore, this work studies the synthesis of silver and gold nanoparticles in batch reactors using constant reactant concentrations, but different process conditions to alter the mass transfer during the synthesis. Silver NPs were synthesized by reduction of silver nitrate *via* sodium borohydride in the presence of trisodium citrate. Gold NPs were synthesized using the Turkevich method, reducing tetrachloroauric acid *via* trisodium citrate. Four synthesis conditions for each NP system were used to investigate the mass transfer effects on the size and dispersity of the NPs. These were the i) slow or ii) fast addition of the concentrated reducing agent to the dilute precursor and the iii) slow and iv) fast addition of the concentrated precursor to dilute reducing agent solutions. Slow addition was performed by adding the reagent dropwise at a rate of 0.5 ml min^{-1} from a tube suspended above the stirred bulk solution, while fast addition was achieved by adding the reagent near the stir bar tip at a rate of 50 ml min^{-1} from a tube submerged in the stirred bulk solution. Mixing times of 209 ms for slow and 46 ms for fast reagent addition were determined using the Villermaux–Dushman protocol in combination with a mixing model. The silver NP size ranged from 6.7 to 11.5 nm for the four mixing conditions tested, with the smallest NPs being synthesized by fast addition of sodium borohydride to a silver nitrate solution. Stabilization of the initially formed particles was key to producing smaller and less polydisperse silver NPs in the case of slow reagent addition. The gold NP size ranged from 13.1 to 18.0 nm, with the smallest NPs being synthesized by fast addition of the trisodium citrate solution to the tetrachloroauric acid precursor solution. Faster reagent addition reduced polydispersity, due to a sharper separation of nucleation and growth. The results for both systems highlight the importance of mass transfer in determining the size and degree of polydispersity in batch synthesis of NPs and indicate that the effects are system-dependent.

Received 19th June 2018,
Accepted 22nd August 2018

DOI: 10.1039/c8ce01014e

rsc.li/crystengcomm

1. Introduction

Noble metal nanoparticles (NPs) offer unique properties as compared to their bulk counterpart, offering potential for a variety of applications. Silver NPs for instance are successfully used in catalysis,[1,2] surface enhanced Raman scattering,[3,4] electronics,[5,6] and as antimicrobial or anti-inflammatory agents[7–10] and sensors.[11,12] Likewise, gold NPs have been utilised for biological/biomedical,[13–18] electrochemical,[19,20] catalytic,[21,22] and optical applications.[23,24] Since the properties of NPs depend on their shape and size (and polydispersity), a well-controlled synthesis is key for satisfactory NP performance.

There are many studies, mostly in batch systems, showing how precursor concentrations and different synthetic conditions (*e.g.*, temperature, synthesis duration, sequence of reagent addition, *etc.*) affect the size of NPs. One factor that is rarely investigated in depth for batch synthesis is mass transfer, *i.e.*, the transport of reagent molecules, particles, volumes of fluid, *etc.*, from one location to another. This is associated with the rate and order of reagent addition and the mixing time. The latter can be categorised into macromixing time, relating to the timescale of bulk homogenization (order of seconds for lab-scale reactors), mesomixing time, relating to the dispersal of reagent plumes, and micromixing time, relating to the molecular diffusion or fluid engulfment on the smallest scales of motion, where flow is no longer turbulent (order of milliseconds)[25,26] Which timescale affects the synthesis does depend on the reaction timescale of the synthesis.[27]

[a] *Department of Chemical Engineering, University College London, Torrington Place, London, WC1E 7JE, UK. E-mail: a.gavriilidis@ucl.ac.uk*
[b] *UCL Healthcare Biomagnetic and Nanomaterials Laboratories, 21 Albemarle Street, London W1S 4BS, UK*
[c] *Biophysics Group, Department of Physics and Astronomy, University College London, Gower Street, London WC1E 6BT, UK. E-mail: ntk.thanh@ucl.ac.uk*
† Electronic supplementary information (ESI) available. See DOI: 10.1039/c8ce01014e

Micromixing times, for example, cannot be neglected for fast reactions, such as the reduction of noble metal precursors by strong reducing agents. It has been shown that with sodium borohydride as the reducing agent precursor reduction is completed within less than 200 ms during the synthesis of gold NPs[28] and similarly in the case of silver NPs.[29,30] The reaction timescale, therefore, is shorter than typical mixing timescale. It is thus essential to understand the effect of mixing conditions on the NP properties to develop scalable batch protocols and reproducible syntheses (not least in different laboratories with varying equipment).

Probably the most common synthesis for silver NPs is the reduction of silver nitrate *via* sodium borohydride and for gold NPs, the Turkevich method, *i.e.*, the reduction of tetrachloroauric acid *via* trisodium citrate at elevated temperatures, which are both studied in this work. However, for both systems there are no benchmark synthesis conditions, including the sequence of reagent addition. In this work we refer to the addition of the reducing agent to a precursor solution as the "standard method", and the addition of the precursor to a reducing agent solution as the "inverse method". The standard method for silver NP synthesis was investigated by Ryu *et al.* Highly concentrated silver NP solutions (up to 40 wt%) with NPs in the range of 1–35 nm were synthesized by reducing ice cold silver nitrate by slow addition of sodium borohydride and/or hydrazine monohydrate in the presence of polyelectrolytes.[31] Pinto *et al.* synthesized silver NPs in the size range of 3–10 nm by the addition of sodium borohydride to a mixture of silver nitrate and trisodium citrate.[32] On increasing the sodium borohydride to silver nitrate molar ratio (by increasing the amount of 1 mM $NaBH_4$ solution added to a 0.25 mM $AgNO_3/Na_3C_6H_5O_7$ solution), the size of the nanoparticles decreased and the concentration of the nanoparticles increased based on UV-Vis spectroscopy analysis. The standard deviation of the absorbance maximum increased with increasing sodium borohydride molar amount, demonstrating lower reproducibility between experiments. Shirtcliffe *et al.* reduced silver nitrate using sodium borohydride and sodium hydroxide using the standard and inverse methods for the synthesis of silver NPs in the range of 15–77 nm.[33] In their work, pipettes were used to mix reagents within a cuvette at 2 °C and it was shown that the method and order of mixing had a significant effect on the NP size distribution. The addition of silver nitrate to a mixture of sodium borohydride and sodium hydroxide produced the narrowest and most reproducible peaks using UV-Vis analysis (though the TEM images showed quite large and polydisperse NPs, possibly because no stabilizer was used in the system).

The inverse method was studied by Song *et al.*[34] Silver NPs between 30 and 40 nm were synthesised by adding silver nitrate to a solution of sodium borohydride and sodium dodecyl sulfate.[34] The authors observed that after exceeding a $[NaBH_4]/[AgNO_3]$ ratio of 5, higher sodium borohydride concentrations resulted in well-dispersed silver NPs. It was suggested that an excess amount of $NaBH_4$ yields a $[BH_4]^-$ ion layer preventing the boron hydroxide (generated due to the hydrolysis of $NaBH_4$), which is assumed to provoke aggregation, from adsorbing onto the surfaces of silver nanoparticles. The fact that sodium borohydride is not only a reducing agent but also a stabilizer is in agreement with the work of Polte *et al.*[29] This detailed study of the silver nanoparticle formation mechanism during the $NaBH_4$ reduction method describes a metastable phase, *i.e.*, particles are stable for several minutes after initial coalescence-based particle growth in the absence of any stabilizer. A subsequent (after ~10 min) decrease of stability, *i.e.*, the continuation of coalescence/aggregation, was suspected to be driven by a changing ratio of $[BH_4]^-/[B(OH)_4]^-$, the increasing pH, or a combination of both. Thøgersen *et al.* synthesized silver NPs between 6–19 nm by slowly dropping an ice cold $AgNO_3$ solution into an ice cold solution of sodium borohydride.[35] They found an increase in NP size due to an increase of the molar ratio of silver nitrate to sodium borohydride. Agnihotri *et al.* synthesized silver NPs in the range of 5–100 nm by adding silver nitrate to a heated solution of sodium borohydride and trisodium citrate (60 °C) and further heating the solution to 90 °C.[36] Monodispersed NPs could be synthesized, which was assigned to a two-step growth mechanism, where sodium borohydride produced small seeds through coalescence of small silver clusters followed by a surface reduction type growth *via* citrate reduction to grow the NPs into a more monodispersed product. The authors were able to synthesize NPs with a wide range of sizes by varying the concentrations of the various components used in the system. In general, altering the ratio of the reducing agent to precursor was the main method to achieve control of the size of the NPs, highlighting the importance of reagent concentration in the resultant silver NP size.

In their original work, Turkevich *et al.* tested a variety of different methods for the synthesis of gold NPs, but found the sodium citrate method to be the most repeatable, typically producing gold NPs in the range between 15 and 20 nm.[37] A minimum size was observed at 80 °C while a lower citrate concentration resulted in an increase in NP size. The standard Turkevich method was later studied by Frens, where gold NPs were synthesised in the range of 12–150 nm by varying the amount of citrate injected into a boiling tetrachloroauric acid solution.[38] The final NP size was found to be determined by the number of nuclei formed (hence, the initial nuclei size), which is why higher amounts of citrate yielded smaller gold NPs. Goodman *et al.* observed a similar trend when increasing citrate concentration, with the gold NP size ranging between 21 and 80 nm.[39] Chow and Zukoski synthesised gold NPs with sizes between 16 and 52 nm for non-agglomerated particles (very large agglomerated NPs were seen in cases where the synthesis of gold NPs did not reach completion).[40] In a recent study, Kettemann *et al.* synthesised gold NPs between 11 and 18 nm using the standard method. A modification in the reducing agent composition was shown to improve the reproducibility of the synthesis significantly.[41]

The inverse method was studied by Sivaraman *et al.*, who synthesised gold NPs in the range of 5–10 nm by adding a small volume of highly concentrated tetrachloroauric solution to a large volume of citrate solution.[42] These authors found that for citrate to gold molar ratios of <5, the mean size of the NPs was not significantly affected whereas for ratios >5, there was a significant reduction in the size of the NPs. Piella *et al.* synthesised monodisperse gold NPs in the range of 3–13 nm based on a modification of the inverse method involving the use of tannic acid together with sodium citrate as the reducing agent.[24] Also Schulz *et al.* synthesized gold NPs of ~12 nm with a low polydispersity of 5–8% using an inverse method.[43]

Ojea-Jiménez *et al.* synthesised gold NPs in the range of 9–37 nm comparing the standard method to the inverse method (swapping the reagent addition order). These authors found that NPs were smaller when tetrachloroauric acid was added to hot citrate.[44] Also Wuithschick *et al.* studied both the standard and inverse methods. Gold NPs were synthesised in the range of 11–42 nm investigating the effect of temperature, ionic strength, pH, variation of reactant concentrations, and the order of reagent addition.[45] The authors' detailed theoretical and experimental work revealed that the final particle size is governed by the size of the initially formed seeds. The seed size itself was shown to depend on the rather complex reduction chemistry and was found to be smaller for the inverse method under the synthesis conditions used. A minimum size was achieved at 60 °C and the synthesis time decreased with increasing temperature. A pH window between 2.8 and 4 was found to produce the lowest polydispersity index of around 10% with the minimum size of 10.8 nm achieved.

The large number of studies on the silver nitrate reduction synthesis by sodium borohydride and the Turkevich method provide an advanced understanding of the mechanisms of these two syntheses providing several options to control the NP size distribution. As shown in this introduction, size control was successfully achieved *e.g.*, by changing reaction temperatures, reactant concentrations, or pH values. Nevertheless, there is a lack of studies which focus specifically on mass transfer and how it affects the resultant NP size and polydispersity. Therefore, this study investigates the two most common methods for the synthesis of silver NPs and gold NPs, with a focus on the role of mass transfer in the resultant size and polydispersity of the respective NP system. Various mixing configurations and orders of addition of the reagents are investigated to study a variety of reaction conditions.

2. Materials and methods

2.1 Chemicals

Silver nitrate ($AgNO_3$, 0.01 M stock solution), trisodium citrate ($(HOC(COONa)(CH_2COONa)_2 \cdot 2H_2O$), powder form), sodium borohydride solution ($NaBH_4$, ~12 wt% in 14 M NaOH stock solution), gold(III) chloride hydrate ($HAuCl_4 \cdot xH_2O$, powder form), potassium iodide (KI, 99%), potassium iodate (KIO_3, 98%) and boric acid (H_3BO_3, 99.5%) were obtained from Sigma Ltd. Sulfuric acid (H_2SO_4, 3 M stock solution) was obtained from Alfa Aesar Ltd. All chemicals were used without further purification and solutions were prepared with ultrapure water (resistivity 15.0 MΩ cm).

2.2 Experimental setup

Syringe pumps (Pump 11 Elite OEM module, Harvard Apparatus) connected to a 0.5 mm internal diameter (I.D.) 316L stainless steel tube for silver NP synthesis and to a 0.5 mm I.D. PTFE tube for gold NP synthesis were used to feed one of the reagents into the batch vessel which was a 50 ml small-neck glass Erlenmeyer flask (Fisher Scientific). A digital hotplate stirrer unit with a temperature controller (Stuart, Cole-Parmer LLC) was used together with PTFE stir bars (15 mm × 1.5 mm) to heat and mix the reagents in the vessel. For the synthesis of gold NPs, a glycerine bath was used to heat the reagents to 80 °C in the batch vessel. A cap, through which the stainless steel or PTFE tube for reagent addition was inserted, covered the vessel. The height of the tube in the vessel could be adjusted to allow addition of reagents above the solution or into the solution near the tip of the magnetic stir bar. Fig. 1 shows a schematic of the experimental setups for silver and gold NP syntheses.

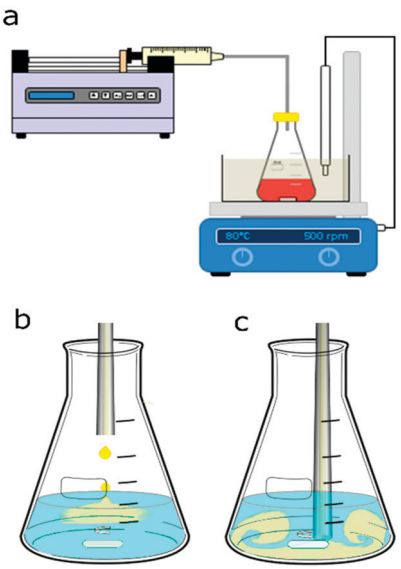

Fig. 1 (a) Schematic of the experimental setup for nanoparticle synthesis consisting of an Erlenmeyer flask with the magnetically stirred precursor or reducing agent solution and a syringe pump delivering the reagent *via* tubing. The setup for gold NP synthesis used a 0.5 mm I.D. PTFE tubing and a glycerine bath in which a temperature probe was immersed to keep the temperature at 80 °C. The setup for silver NP synthesis used a stainless steel 0.5 mm I.D. tubing at room temperature. The stirrer speed was set to 500 rpm in both cases. Two injection points within the vessel were chosen for the different mixing conditions. Reagents were fed to the vessel either (b) above the solution or (c) close to the stir bar tip. In the latter case a small air gap was introduced at the tubing outlet to avoid contact of the reagent solutions before the synthesis was started.

2.3 Nanoparticle synthesis conditions

For the silver NP syntheses, 20 ml of one reagent were placed in the batch vessel and stirred at 500 rpm. To this reagent solution, 0.6 ml of the other reagent was added *via* the syringe pump either dropwise at 0.5 ml min^{-1} above the solution through a stainless-steel tube, see Fig. 1b, or at once with a feed rate of 50 ml min^{-1} through the tube inserted into the solution within the vessel near the stir bar tip, as shown in Fig. 1c. The reagents were a silver nitrate solution with trisodium citrate serving as a capping agent (the precursor solution) and a sodium borohydride solution (the reducing agent solution). Sodium borohydride was stored in 14 M sodium hydroxide (as received) leading to a NaOH concentration being 3.21 times higher than the sodium borohydride concentration in all silver NP syntheses. The order of reagent addition was tested by switching which reagent was initially placed in the batch vessel, either 20 ml of the precursor solution or 20 ml of the sodium borohydride solution, to which then 0.6 ml of the other reagent was fed. The concentrations of the reagent initially placed in the vessel and the fed reagent were changed based on their volumes, to have equal nominal concentrations after mixing. Details of used concentrations for the silver NP synthesis are provided in section 3.1.

Similarly, for the gold NP syntheses, 20 ml of one reagent was placed in the batch vessel and 0.6 ml of the other reagent was added through PTFE tubing. Either 20 ml of tetrachloroauric acid solution (the precursor solution) or 20 ml of trisodium citrate (the reducing agent solution) were initially placed in the batch vessel. The vessel was placed in the glycerine bath which was heated to 80 °C. To test how long it takes to heat 20 ml of solution to 80 °C, the temperature was measured over time after inserting the solution at room temperature into the glycerine bath. For all cases, 7 min was sufficient to reach the steady state of 80 °C. The reagent solution in the vessel was always kept at this temperature under stirring for 15 min before the addition of 0.6 ml of the other reagent. Details of used concentrations for the gold NP synthesis are provided in section 3.2.

2.4 Characterization of nanoparticles

NPs were analysed using a UV-Vis spectrometer (USB 2000+ spectrometer and DT-Mini-2-GS light source, Ocean Optics). Silver NPs were analysed within an hour of synthesis (the signal of the samples was stable in this time window). Gold NPs were analysed over time till the signal had stabilized (usually 1–2 days). The shown UV-Vis results from gold NPs relate to stabilized samples only. NP samples were diluted with additional ultrapure water to be in the linear absorbance range. Online UV-Vis measurements using the same spectrometer during the synthesis of silver NPs were implemented by recirculating the solution from the reaction vessel *via* a peristaltic pump and passing it through a UV-Vis flow cell (details are shown in the ESI,† section 5). Transmission electron microscopy (TEM) images were captured using a JEOL 1200 EX microscope with an acceleration voltage of 120 kV. The samples were prepared within an hour of the synthesis completion for silver NPs and when the sample was stable for gold NPs by pipetting 5 μl of the sample onto carbon coated copper TEM grids, which were allowed to dry at room temperature. Particle size distributions (insets for each TEM image presented) have the following nomenclature: d is the average diameter, δd is the standard deviation of the NP size distribution and n is the number of particles counted to obtain the particle size distribution. Dynamic light scattering (DLS) size and zeta potential measurements were performed with a DelsaMax-Pro (Beckman Coulter) using the available flow cell system in batch mode at 22 °C. DLS measurements were performed at least five times, with a data acquisition time of 10 s.

2.5 Mixing characterization

Characterization of mixing within the batch vessel was carried out using the Villermaux–Dushman reaction scheme. In this reaction system, sulfuric acid is added to a buffer solution consisting of a mixture of orthoboric acid, sodium hydroxide, potassium iodide and potassium iodate ions. The reaction scheme of the Villermaux–Dushman protocol is as follows:

$$H_2BO_3^- + H^+ \leftrightarrow H_3BO_3 \quad (1)$$

$$5I^- + IO_3^- + 6H^+ \leftrightarrow 3I_2 + 3H_2O \quad (2)$$

Reactions (1) and (2) compete for protons supplied by the sulfuric acid. The neutralization reaction of dihydrogen borate (1) is considered to be instantaneous, while reaction (2), which yields iodine, is fast but slower than reaction (1). Therefore, in the limit of instantaneous mixing, only reaction (1) occurs. Slower mixing results in local depletion of dihydrogen borate, thus allowing reaction (2) to occur. The selectivity of this reaction scheme therefore relates to the micromixing (and mesomixing) timescale. The generated iodine can then be quantified, since it reacts in an equilibrium reaction (3) with excess iodide to triiodide.

$$I_2 + I^- \leftrightarrow I_3^- \quad (3)$$

The triiodide concentration can be easily quantified due to its absorption in the UV-Vis-range, typically at a wavelength of 353 nm. Its value allows determination of the degree of mixing efficiency, which is related to the extent to which reaction (2) has occurred. Once the selectivity of the reaction scheme is known, the order of magnitude of the mixing time can be estimated using a mixing model.

The mixing model is required to relate the triiodide concentration (= model output), which depends on the initial concentrations of sulfuric acid, orthoboric acid, sodium hydroxide, potassium iodide and potassium iodate (= model inputs), to the mixing time (= model variable). In this study,

the interaction by exchange with the mean (IEM) mixing model was used. For the mixing experiments, 1 ml of 0.14 N sulfuric acid was added to 20 ml of a buffer solution consisting of 181.8 mM orthoboric acid, 90.9 mM sodium hydroxide, 11.67 mM potassium iodide and 2.33 mM potassium iodate. The stirrer speed was set to 500 rpm (as used for all syntheses) and the two mixing configurations used in the NP synthesis were tested, *i.e.*, acid was injected from the centre above the buffer solution or near the stir bar tip. Fig. 1b and c show the schematics of the two configurations. The final triiodide concentration was obtained using an extinction coefficient of 23 209 l mol^{-1} cm^{-1}. This extinction coefficient was determined using solutions of a known iodine concentration as described in the ESI,† section 1. Experiments were repeated three times for each mixing configuration. The mixing time averaged over the three repetitions was 209 ms for the dropwise injection above the solution and 46 ms in the case of injection near the stir bar tip. Details on the mixing model used to assign the mixing time values to the measured triiodide concentrations are provided in the ESI,† section 2. The measured reduction in the mixing time when injecting near the stir bar tip was expected because of the higher shear rates near the stir bar tip and the high flow rate (50 ml min^{-1}) used for the addition.

3. Results and discussion

3.1 Silver nanoparticle synthesis

Silver NPs were synthesized in the batch vessel by the reduction of silver nitrate *via* sodium borohydride in the presence of the stabilizer trisodium citrate. The effect of changing a) the mixing configuration and b) the order of reagent addition (swapping the reagent placed in the batch vessel) on the size and polydispersity of the NPs was investigated. As described above, for all syntheses 20 ml of one reagent was stirred in the batch vessel while feeding 0.6 ml of the second reagent into the vessel *via* the stainless-steel tubing. Hence, four different syntheses were performed, which we refer to as Ag-R-s, Ag-R-f, Ag-P-s, and Ag-P-f. R and P refer to the order of reagent addition: R is for adding reducing agent solution, while P is for adding precursor solution. The mixing configurations are denoted by the letters s (slow) and f (fast). Slow (*i.e.*, slow addition) is for the reagent added dropwise at a rate of 0.5 ml min^{-1} from above, while fast (*i.e.*, fast addition) is for the reagent added quickly near the stir bar tip with a feed rate of 50 ml min^{-1}. For example, the synthesis condition Ag-R-s describes the addition of 0.6 ml of the reducing agent at a rate of 0.5 ml min^{-1} to 20 ml of precursor solution. Table 1 summarizes the concentrations for each mixing condition (5 to 1 molar ratio of sodium borohydride to silver nitrate was used in all cases). The precursor concentrations of the conditions Ag-P-s and Ag-P-f had to be chosen slightly lower due to the low concentration of the (as received) silver nitrate solution and the solubility of sodium citrate in aqueous solutions, limiting the maximal concentrations of the precursor solution to 9.1 mM.

UV-Vis spectroscopy performed subsequent to the synthesis (>20 min after feeding of the precursor or reducing agent solution was completed) showed a surface plasmon absorption peak at 387.3 nm, 388.5 nm, 388.8 nm, and 388.6 nm for the conditions Ag-R-s, Ag-R-f, Ag-P-s, and Ag-P-f, respectively. The syntheses Ag-P-s and Ag-R-f exhibited a significantly higher reproducibility in terms of the surface plasmon peak position (lower standard deviation, experiments performed in triplicate) than the syntheses Ag-R-s and Ag-P-f. The details of this UV-Vis analysis, including a comparison of the absorbance values, are summarized in Fig. S4.† Fig. 2 shows the TEM images of the synthesized silver NPs exhibiting an average particle diameter of 11.1 ± 3.0 nm, 6.7 ± 1.7 nm, 9.5 ± 1.4 nm, and 11.5 ± 2.4 nm for the conditions Ag-R-s, Ag-R-f, Ag-P-s and Ag-P-f, respectively. The difference in the NP diameters obtained from the TEM studies is statistically significant comparing all four synthesis conditions (*i.e.*, six combinations) *via* an unpaired *t*-test and Welch's unpaired *t*-test (assuming unequal sample variances) with a 5% significance level. Due to the large number of analysed particles, even the diameters for the conditions Ag-R-s and Ag-P-f were found to be statistically different.

Comparison between Ag-R-s and Ag-P-s synthesis conditions. To study the difference in the reaction kinetics of the Ag-R-s and Ag-P-s syntheses, additional online UV-Vis spectroscopy studies were performed. Absorption spectra were recorded every second and a spectrum recorded before the start of the addition of the reducing agent (Ag-R-s) or precursor solution (Ag-P-s) was used as the reference. The immediate increase in absorption during the synthesis Ag-R-s (see Fig. 3a), *i.e.*, the dropwise addition of the reducing agent to the precursor solution over 72 s, shows that even a small fraction of the reducing agent was sufficient to reduce almost all $AgNO_3$. After about 4 s changes in absorbance became marginal. It should be mentioned that, due to the residence time of solution in the tubing to the UV-Vis flow cell, there was a delay of a few seconds which somewhat limited the time resolution of these measurements.

Table 1 Summary of silver NP synthesis conditions, listing the volumes and concentrations of the reducing agent solution (sodium borohydride, $NaBH_4$) and precursor solution (silver nitrate, $AgNO_3$) with the capping agent (trisodium citrate, $Na_3C_6H_5O_7$), as well as their nominal concentrations after mixing

Condition	Reducing agent	Volume	Conc. after mixing	Precursor/capping agent	Volume	Conc. after mixing
Ag-R-s	63.3 mM	0.6 ml	1.84 mM	0.38/0.38 mM	20 ml	0.37/0.37 mM
Ag-R-f	63.3 mM	0.6 ml	1.84 mM	0.38/0.38 mM	20 ml	0.37/0.37 mM
Ag-P-s	1.36 mM	20 ml	1.32 mM	9.1/9.1 mM	0.6 ml	0.27/0.27 mM
Ag-P-f	1.36 mM	20 ml	1.32 mM	9.1/9.1 mM	0.6 ml	0.27/0.27 mM

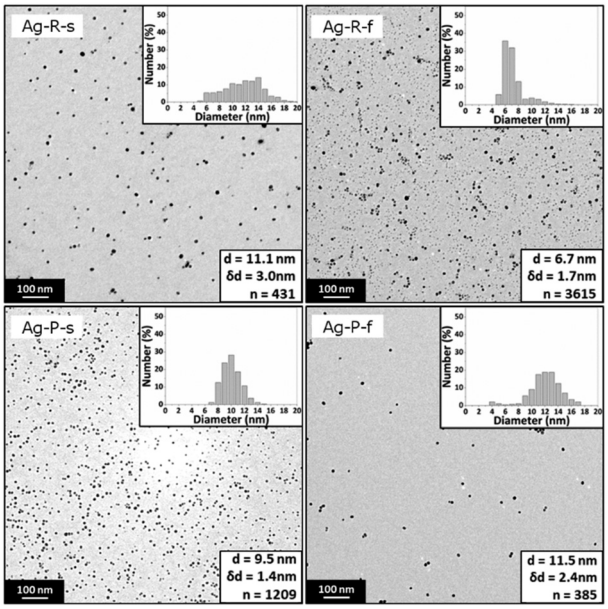

Fig. 2 Representative TEM images and statistics of silver NPs synthesized *via* the four synthesis conditions Ag-R-s, Ag-R-f, Ag-P-s, and Ag-P-f. Details of these conditions are listed in Table 1.

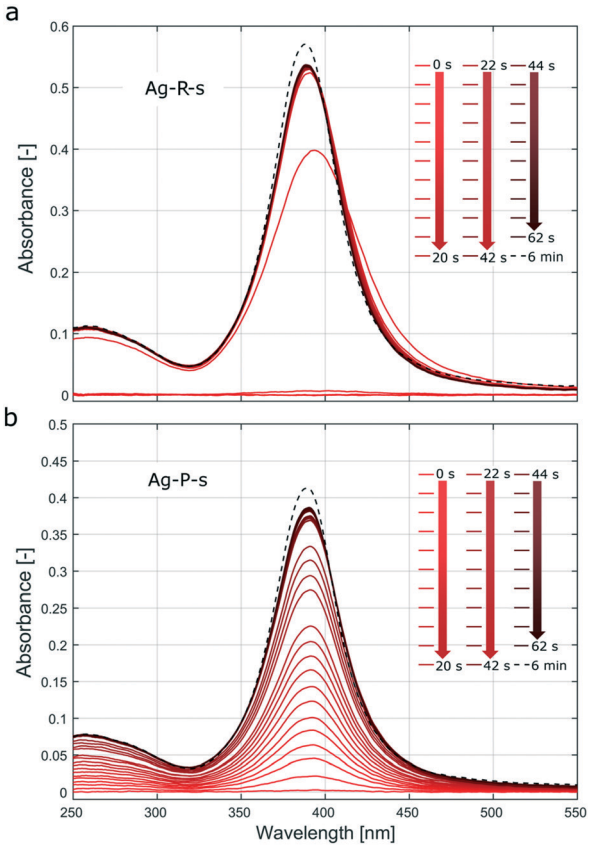

Fig. 3 UV-Vis spectra recorded during the silver NP syntheses (a) Ag-R-s and (b) Ag-P-s. The solid lines show the spectra during the first 62 s after the onset of reagent addition (every second spectra plotted, *i.e.*, 2 s interval). The dashed lines show the spectrum after 6 min, *i.e.*, ~5 min after complete addition of the 0.6 ml solution. Due to the residence time of the solution in the tubing used for the online UV-Vis spectroscopy setup, there is a lag of approximately 3 s between the start of the reaction and the passing of the solution from the vessel through the flow cell.

Fig. S7† showing UV-Vis spectra recorded during stepwise addition of the reducing agent, as described in section 5 of the ESI,† indicates that the particle formation was almost complete (not referring to morphological changes) after adding <20% of the final amount. In Fig. 3a, the UV-Vis spectra recorded during the first 5–10 s exhibit a shift of the surface plasmon absorption band to longer wavelengths compared to the subsequent spectra. This could be assigned to aggregated particles during the initial phase or a decrease of the electron density on the silver NP surface upon chemisorption of Ag^+ as described, *e.g.*, by Henglein *et al.*[46] These authors reported a significant shift to larger wavelengths for Ag^+ concentrations that were two orders of magnitude lower than the $AgNO_3$ concentration used in Ag-R-s. Video analysis of the synthesis Ag-R-s showed a dark brown plume immediately on addition of the first drop of sodium borohydride solution, which then turned to a bright yellow colour (videos of all silver syntheses can be downloaded from the journal's website). This immediate reduction during Ag-R-s, as confirmed *via* video and online UV-Vis studies, is not surprising, as sodium borohydride is known to have the potential to reduce more than its own stoichiometric equivalent of silver ions, since it can provide multiple electrons in the reduction reaction.[47–49] Hence, for Ag-R-s most of the silver precursor was reduced with the first drops of the reducing agent solution (*i.e.*, the first ~0.01 ml and a molar ratio of $AgNO_3$/$NaBH_4$ ~12).

In contrast, Fig. 3b (and Fig. S8,† showing UV-Vis spectra during stepwise addition of the precursor solution) shows that the absorption during the synthesis Ag-P-s increased in proportion to the quantity of added precursor solution. This indicates that the particles that precipitated after the first drop of precursor solution was added had similar absorption (here not distinguished from scattering) properties to those formed after addition of the last drop. As the precursor solution was added dropwise, the synthesis Ag-P-s did not allow a large amount of $AgNO_3$ to be reduced at the same time (and space). The UV-Vis results suggest that each drop of silver nitrate reacted to form silver NPs within seconds, which were then distributed in the sodium borohydride solution. Further drops then produce new NPs which are distributed again over the vessel before the next drop arrives. The stepwise addition of the precursor solution, as during Ag-P-s, does make seed mediated growth more likely (further precursor addition and reduction on the surface of initially formed particles) compared to Ag-R-s, where most of the precursor is reduced at once leading to burst nucleation (no further growth of initially nucleated particles due to lack of unconsumed precursor).

One of the biggest differences between these syntheses was that in the case of Ag-R-s all the precursor was reduced within seconds resulting in a temporarily high release of the

silver precursor compared to Ag-P-s where the fed precursor was reduced throughout the feeding time of 72 s. The other difference was that particles synthesized *via* Ag-R-s were not exposed to the final sodium borohydride concentration from the first drop, as was the case for the condition Ag-P-s. Since sodium borohydride also acts as a stabilizing agent,[34,50] Ag-R-s can be expected to provoke agglomeration, especially during the initial phase of the synthesis (at lower sodium borohydride concentrations). Although the precursor solution did contain the capping agent trisodium citrate, the latter might not stabilize the just formed nanoparticles sufficiently against agglomeration.

Aggregation has been identified in previous studies as the main growth mechanism in the silver NP formation process using sodium borohydride reduction[29,51,52] and recent publications suggest that electrostatic repulsion forces (also referred to as the aggregation barrier[53] in combination with particle size) determine up to which aggregation size of metal NPs is possible, hence the final NP size. The lower concentrations of sodium borohydride during the initial phase would explain the initially lower aggregation barrier during Ag-R-s (when most if not all of the precursor was already reduced), yielding larger particles than those in the synthesis Ag-P-s (exhibiting a high sodium borohydride concentration throughout the synthesis and gradual reduction of the precursor). This is in agreement with the larger particle diameter and higher polydispersity observed for Ag-R-s.

To obtain more information on the silver NP formation mechanism during the synthesis Ag-R-s, a TEM sample was prepared immediately (<2 min) after the addition of only 0.02 ml sodium borohydride solution *via* an Eppendorf pipette (=3.3% of the final reducing agent solution, *i.e.*, a molar ratio of $AgNO_3/NaBH_4$ = 6 after mixing). The TEM images in Fig. 4 show bigger particles than those synthesized *via* the original condition Ag-R-s, indicating reduced stabilization due to the lower sodium borohydride concentration.

Comparison between Ag-R-f and Ag-P-f synthesis conditions. Assuming instantaneous mixing, the reaction conditions for Ag-R-f and Ag-P-f should have been similar (despite the slight discrepancy in the final precursor concentration, see Table 1), and so should be the final silver NP size distributions. However, the discrepancy in the particle size shows that this is not the case. Obviously, the particle formation was faster than the mixing time of 46 ms, for at least one of these two fast mixing conditions. Following the previous argument of stabilization with $NaBH_4$, this difference in size cannot be explained by the effectiveness of stabilization of the initially formed particles. As discussed before comparing Ag-R-f and Ag-P-s (the difference in the initial sodium borohydride concentrations was considered to effect the aggregation barrier), since the $[BH_4]^-/[AgNO_3]$ ratio was almost the same. However, local mixing phenomena cannot be excluded, since the (micro)mixing time (46 ms) is only one order of magnitude smaller than the time needed for the addition of the second reagent in the case of Ag-P-f (720 ms).

In experiment Ag-R-f, concentrated sodium borohydride solution was added quickly to a dilute precursor solution. Based on the video and UV-Vis analysis for Ag-R-s showing the immediate reduction of all the precursor with just a fraction of the reducing agent solution, this synthesis condition is expected to cause a faster reduction of the precursor resulting in higher nucleation rates. Since mixing times are fast, nucleation events are not restricted to a confined space. This limits the number of NP collisions and hence possible aggregation events during the initial particle formation phase. This also explains the large difference in the silver NP size and polydispersity between the syntheses Ag-R-s and Ag-R-f.

In experiment Ag-P-f, concentrated precursor solution was added quickly to a sodium borohydride solution. Assuming that the reaction kinetics was faster than the time needed for the addition of the precursor solution (which could be expected as discussed by Polte *et al.*[29]), the reduction and hence nucleation rates would be slower than those for Ag-R-f (where all the precursor was available for reduction at the start of the synthesis) and nucleation and growth was favoured to occur simultaneously. This agrees with the larger particles observed for Ag-P-f, compared to those for Ag-R-f. For Ag-P-f and Ag-P-s silver NP sizes were comparable.

Stabilization dynamics. To study the stabilization kinetics, the temporal behaviour of the size and zeta potential was recorded over time after each synthesis by DLS, see Fig. 5 and Fig. S9.† Samples (~2 ml) were withdrawn from the vessel 5, 20, 25 and 30 min after the synthesis, *i.e.* complete addition of the 0.6 ml feed solution. These studies showed that zeta potential values can change distinctly with time after synthesis, indicating changes in the NP surface chemistry, possibly because of trisodium citrate adsorption. A change in the surface chemistry of initially formed NPs over time was observed by other authors as well.[29,54] Polte *et al.* discussed the hydrolysis of sodium borohydride attached to silver NPs after 5–90 min (depending on whether additional stabilizers, apart from sodium borohydride, were present; the synthesis was performed with and without additional stabilizers). The transition of $[BH_4]^-$ to $[B(OH)_4]^-$ was described to result in further aggregation and hence a second growth step yielding an increase in the mean diameter from 2–5 nm to the final

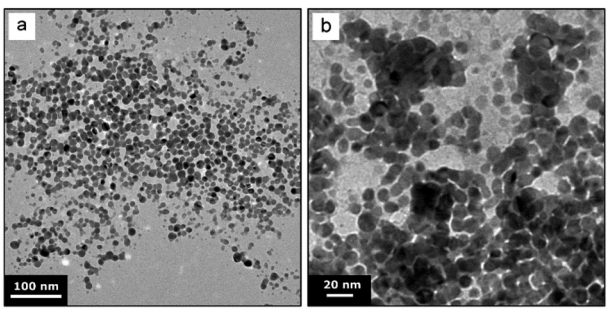

Fig. 4 TEM images of silver NPs synthesized similarly to the experiment Ag-R-s, but adding only 0.02 ml of the sodium borohydride solution [63.3 mM], *i.e.*, 3.3% of the 0.6 ml added during the original synthesis: (a) overview and (b) higher magnification image.

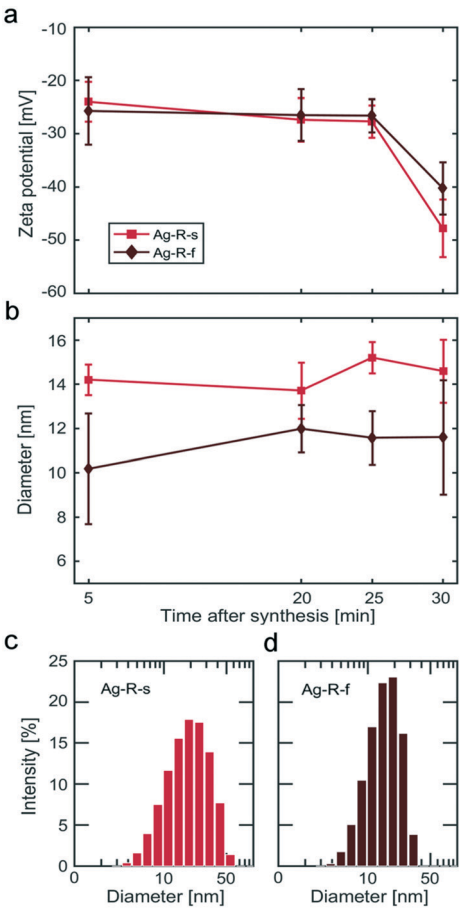

Fig. 5 Silver NP characteristics obtained by DLS after the Ag-R-s and Ag-R-f syntheses. Temporal behaviour of (a) the zeta potential and (b) intensity weighted diameter after completing the addition of the reducing agent or precursor solution. The error bars show the standard deviation of the five measurements performed for each sample. Size distributions as obtained *via* DLS for the samples taken after 30 min: (c) Ag-R-s and (d) Ag-R-f.

NP size of approximately 10 nm. However, a change in the stabilization chemistry that would reduce the aggregation barrier is not in agreement with the observed increase in the magnitude of the zeta potential values after ~25 min (see Fig. 5). Ag-R-s and Ag-R-f reached zeta potential values associated with efficient stabilization (>|−40| mV) after 30 min starting from −22 to −23 mV determined 5 min after the synthesis. This could be assigned to the stabilization by trisodium citrate during that time span. The second growth step discussed by Polte *et al.* (not only for Ag NPs but also for Cu and Pd NPs synthesized by sodium borohydride reduction) might have occurred at an earlier stage, *i.e.*, before the first zeta potential measurement. The sizes of silver NPs synthesized in Ag-R-s and Ag-R-f, obtained by DLS, were in good agreement with TEM data, *i.e.*, 14.6 ± 2.6 nm and 11.6 ± 2.6 nm (see Fig. 5, 30 min). It should be noted that DLS measures the hydrodynamic diameter in contrast to core-size by TEM, which is why sizes determined by DLS are larger. Furthermore, DLS is more sensitive towards larger particles as light scattering scales with particle size to a power of 6.

For the Ag-P-s and Ag-P-f syntheses, the DLS studies revealed particles in solution which were distinctly larger (>100 nm) than those determined from TEM images, see Fig. S9.† However, particles >100 nm were not silver NPs, since such large silver NPs would have affected significantly the TEM data and the UV-Vis spectra, which was not the case. For example, the surface plasmon absorption band would peak at around 450 nm, even for 60 nm particles.[55] Therefore, the large particles measured *via* DLS analysis for Ag-P-s and Ag-P-f, *i.e.*, when feeding highly concentrated $AgNO_3$/$Na_3C_6H_5O_7$, are assigned to larger aggregates (not necessarily silver NPs, probably silver citrate precipitates formed in the precursor solution) present during these syntheses. Further UV-Vis and DLS studies during the preparation of the precursor solution for Ag-P-s and Ag-P-f showed a clear increase in absorption and the occurrence of a particulate phase of unknown composition with particles >100 nm as soon as the trisodium citrate solution was added to the silver nitrate solution (data not shown). This indicates precipitation in the precursor solution at high silver nitrate and trisodium citrate concentrations.

3.2 Gold nanoparticle synthesis

The effect of changing the mixing configuration and the order of reagent addition on the size and polydispersity of the gold NPs was investigated. The same four conditions as those used for silver NP synthesis were tested and described as conditions Au-R-s, Au-R-f, Au-P-s and Au-P-f. Table 2 summarizes the concentrations and fed volumes for each mixing condition (a citrate/tetrachloroauric ratio of 5 : 1 was used in all four syntheses).

UV-Vis spectroscopy studies showed a surface plasmon absorption peak at 523.3 nm, 521.0 nm, 522.5 nm, and 521.6 nm for the conditions Au-R-s, Au-R-f, Au-P-s, and Au-P-f. The Au-P-f synthesis exhibited the highest reproducibility, when the surface plasmon peak position and absorbance were compared. The details of this UV-Vis analysis are summarized in Fig. S5.† Fig. 6 shows the TEM images of the synthesized gold NPs with an average diameter of 18.0 ± 4.8 nm, 13.1 ± 2.2 nm, 16.3 ± 3.3 nm and 16.2 ± 2.1 nm for conditions Au-R-s, Au-R-f, Au-P-s, and Au-P-f, respectively. The difference in gold NP diameters obtained from TEM studies is statistically significant comparing all four synthesis conditions *via* an unpaired *t*-test and Welch's unpaired *t*-test with a 5% significance level, except for the Au-P-s and Au-P-f conditions.

The largest and most polydisperse NPs were observed for the synthesis Au-R-s and the smallest NPs were observed *via* Au-R-f. Conditions Au-P-s and Au-P-f produced NPs of similar size, though Au-P-f produced more monodisperse gold NPs. Recent studies on the Turkevich synthesis method revealed its seed-mediated growth mechanism, which differs not only from the classical "nucleation–growth" mechanism, but also from the colloidal growth mechanism of the discussed silver NP syntheses using sodium borohydride as the reducing agent. The current understanding of particle formation

Table 2 Summary of gold NP synthesis conditions, listing volumes and concentrations of the reducing agent solution (trisodium citrate, $Na_3C_6H_5O_7$) and the precursor solution (tetrachloroauric acid, $HAuCl_4$), as well as their nominal concentrations after mixing

Condition	Reducing agent/capping agent	Volume	Conc. after mixing	Precursor	Volume	Conc. after mixing
Au-R-s	92.7 mM	0.6 ml	2.70 mM	0.56 mM	20 ml	0.54 mM
Au-R-f	92.7 mM	0.6 ml	2.70 mM	0.56 mM	20 ml	0.54 mM
Au-P-s	2.78 mM	20 ml	2.70 mM	18.5 mM	0.6 ml	0.54 mM
Au-P-f	2.78 mM	20 ml	2.70 mM	18.5 mM	0.6 ml	0.54 mM

during the Turkevich synthesis is that the initial reduction of the precursor is followed by the formation of stable seed particles of a few nm in diameter onto which remaining gold ions attach, making the nanoparticles grow.[45,56] This mechanism is not intuitive since the separation of nucleation and growth, yielding the monodisperse gold NPs the Turkevich synthesis is known for, originates from the reduction of precursor reactivity just after seed formation. However, also in the case of the Turkevich synthesis, the final particle size is determined during the initial stages of the synthesis, *i.e.*, by the size of formed seeds.

Comparison between Au-R-s and Au-P-s synthesis conditions. The conditions Au-R-s and Au-P-s produced NPs of similar size, with Au-R-s yielding the largest particles. This agrees with the longer wavelength of the surface plasmon peak. In addition, Au-R-s exhibited the lowest reproducibility, *i.e.*, the highest standard deviation of the wavelength of the surface plasmon absorption peak, obtained when each condition was repeated in triplicate. The reaction chemistry of the Turkevich method is rather complex because the reactants (citrate and gold ions) can coexist in different forms not only as the synthesis proceeds, but also in the starting solutions. As mentioned above, the separation of nucleation and growth (which leads to the synthesis of monodisperse particles) is due to the reduction of precursor reactivity just after seed formation. The gold precursor is known to exist in increasingly hydroxylated forms, from $AuCl_4^-$ to $Au(OH)_4^-$ (and the intermediates $AuCl_{4-x}(OH)_x^-$) with increasing pH value.[57] According to the literature, an increase in the hydroxylation level results in a decrease in reactivity, and the most reactive species $AuCl_4^-$ exists only during the initial stage of the synthesis (in the case of classic/direct Turkevich synthesis), since the addition of citrate solution causes an increase in pH.[45] Also the speciation of citrate is dependent on the pH value. At lower pH it exists in its most protonated form of H_3Cit with increasing deprotonation to Cit^{3-} as the pH increases, while the $CitH^{2-}$ species is suggested to be the most likely form responsible for the reduction of the gold precursor by Kettemann *et al.*[41] However, $CitH_2^-$ has also been suggested.[58]

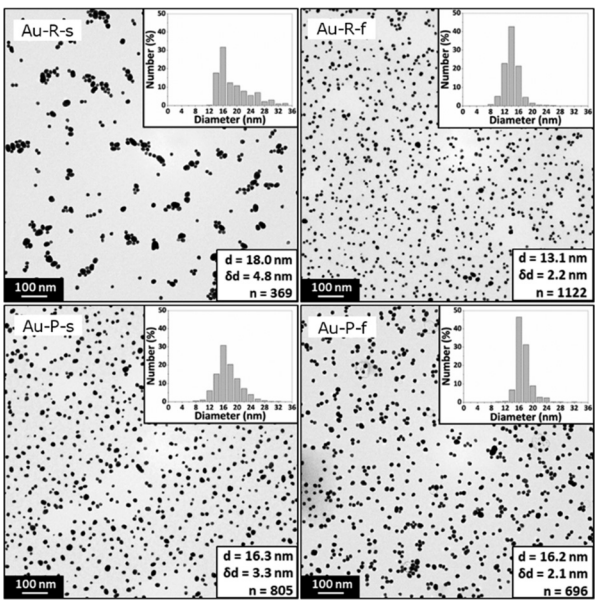

Fig. 6 Representative TEM images and statistics of gold NPs synthesized *via* the four synthesis conditions Au-R-s, Au-R-f, Au-P-s, and Au-P-f. Details of these conditions are listed in Table 2.

The timescale required to finish seed formation, *i.e.*, the step determining the final NP size, was reported to be in the order of 20 s.[45] Although the timescales are dependent on the precursor and citrate concentrations, temperature and pH values, it is obvious that a feeding time of 72 s (as in the case of Ag-R-s and Ag-P-s) hinders a clear separation of nucleation from growth. This is in agreement with our results showing higher polydispersity for slow mixing conditions compared to the fast mixing conditions. Other studies indicate the benefit of fast mixing during the (inverse) Turkevich synthesis for the generation of monodisperse NPs as well.[43] This is consistent with the more monodisperse particles synthesized *via* Au-P-s.

Comparison between Au-R-f and Au-P-f synthesis conditions. Assuming perfect mixing for the Au-R-f and Au-P-f syntheses, *i.e.*, good mixing conditions after instantaneous reagent addition, and the chemistry of the reagents to be identical, the reaction conditions for the Au-R-f and Au-P-f syntheses should yield identical gold NP size distributions. However, NPs synthesized with the condition Au-R-f were statistically smaller than those synthesized with Au-P-f, even if this difference was small (~3 nm). UV-Vis studies showed very good reproducibility for both experiments. It is noteworthy that this was not the case for the silver NP syntheses using fast mixing conditions, in which a strong reducing agent was used, as discussed above. In the case of the Turkevich synthesis, this discrepancy in particle size for syntheses performed at identical nominal concentrations after mixing does not necessarily indicate that particle formation (seed generation) is faster than the mixing time (46 ms). As discussed above, the reaction chemistry of the solutions is

complex and different process settings (*e.g.*, high temperature, low pH value) can have opposing effects on the precursor or citrate reactivity.

Besides the pH, higher temperatures are known to shift the equilibrium of the gold precursor towards more hydroxylated forms as well. The effect of temperature on the citrate solution is not yet clear, but irreversible changes (based on UV-Vis spectroscopy) have been reported during heating which could be explained by the oxidation of citrate *e.g.*, to dicarboxyacetone (DCA).[45] The role of DCA is controversial in the literature. It has been postulated that the inverse method yields smaller (and more monodisperse) particles because the preheated citrate solution forms the more reactive species DCA, which therefore increases the nucleation rate.[43,44] However, studies by Wuithschnick *et al.* performing the Turkevich synthesis adding high concentrations of DCA to the citrate solution (1 mM) prior to the synthesis showed no significant influence of DCA on the particle size. The authors attributed the smaller particles synthesized *via* the inverse Turkevich synthesis to different initial amounts of the reactive $AuCl_4^-$ species and argued that when the inverse method was used, the precursor solution had a higher tetrachloroauric acid concentration (as was the case in this work, see Table 2) and was kept at room temperature before addition. Both would shift the $AuCl_{4-x}(OH)_x^-$ speciation equilibrium towards the most reactive $AuCl_4^-$ species, *i.e.*, the least hydroxylated form. Therefore, one can assume that for the inverse method, the nucleation rate is higher and the seed particles are smaller. However, this line of reasoning is slightly controversial, since similar argumentation would be possible discussing the higher pH of the precursor solution in the vessel (in the case of Au-R-f) in combination with the mixing kinetics.

For the condition Au-R-f, reactive species in the precursor solution in the vessel might remain sufficiently low to suppress nucleation during the initial stages of mixing with the reducing agent, *i.e.*, mixing comes closer to completion before the onset of nucleation, which could yield higher nucleation rates later and hence smaller NPs. In comparison, nucleation is expected to occur throughout the addition of the precursor solution in the case of Au-P-f. In any case, a discussion solely based on the $AuCl_4^-$ concentrations is insufficient, since the interaction between the precursor and the citrate (and all their possible complexes) needs to be taken into consideration, and both reaction temperature and precursor solution pH do not have a monotonic effect on the particle size and polydispersity.

It is very complex to identify the intermediates involved in the reduction mechanism during the very first seconds of reagent mixing. Although timescales in the range of seconds have been reported, *e.g.*, for the equilibration of the $AuCl_{4-x}(OH)_x^-$ species, kinetic data of the reduction are scarce. Our results show that mixing times, even in the order of milliseconds, cannot be neglected for the discussion of the final NP sizes. Although for the slow mixing conditions the inverse method (Au-P-s) produced smaller particles than the direct method (Au-R-s), the trend was reversed for the fast mixing conditions. Our results do not indicate higher reduction rates, and therefore higher nucleation rates and smaller NPs, due to intermediates formed in the citrate solution formed at elevated temperatures. The reversed trend, *i.e.*, larger particle sizes in the case of the inverse method with fast mixing, was unexpected based on previous studies. However, it is worth noting that Sivaraman *et al.* reported the difference in the size of NPs synthesized by the inverse and direct methods to vanish for higher tetrachloroauric acid concentrations (at concentrations higher than 0.54 mM used in this study).[42]

4. Summary and conclusions

Mixing times in a batch vessel were characterized using the Villermaux–Dushman reaction system for two different mixing conditions: 1) dropwise injection of the reagent above the stirred solution in the batch vessel and 2) rapid injection of the reagent near the stir bar tip. The (micro)mixing times were found to be 209 ms when reagents were injected from above and 46 ms when they were injected near the stir bar tip. Silver NPs were synthesized by reducing silver nitrate with sodium borohydride in the presence of trisodium citrate (the stabiliser) under both mixing conditions and different orders of reagent addition, *i.e.*, four different synthesis conditions. It was found that the addition of sodium borohydride at a fast rate near the stir bar tip produced the smallest NPs (6.7 ± 1.7 nm). Slightly bigger but more monodisperse silver NPs (9.5 ± 1.4 nm) were produced by dropwise addition of the precursor solution into the reducing agent solution. Larger and more polydisperse NPs were synthesized when the mixing conditions encouraged lower sodium borohydride concentrations. Online UV-Vis studies showed that complete precursor reduction occurred within seconds, even after adding just a small fraction (<20%) of the final reducing agent solution (final $NaBH_4$: $AgNO_3$ ratio was 5 : 1). Dynamic zeta potential studies showed a second state of stabilization, *i.e.*, a further increase in the magnitude of the zeta potential ~30 min after the complete addition of the second reagent. This indicates a stabilization process that is significantly slower (hours) than the formation of particles (seconds).

Gold NPs were synthesized using the Turkevich method, where tetrachloroauric acid was reduced by trisodium citrate at an elevated temperature. Again, four different syntheses were tested, *i.e.*, two mixing conditions and different orders of reagent addition. Using the same mixing configurations as those for the silver NP synthesis, the smallest NPs (13.1 ± 2.2 nm) were obtained when the reducing agent (trisodium citrate) was added to the precursor (tetrachloroauric acid) at a fast rate near the stir bar tip. These were significantly smaller than when the trisodium citrate was added at a slow rate from above the solution (18 ± 4.8 nm). For both orders of reagent addition, NP polydispersity was significantly lower for the fast mixing conditions, showing the importance of mixing for the Turkevich synthesis. For the fast addition of a concentrated precursor solution to a reservoir of preheated

citric acid solution (16.2 ± 2.1 nm) a polydispersity of <8% could be achieved. Although the inverse method, *i.e.* adding the tetrachloroauric acid solution to the citrate solution, was reported to produce smaller and more monodisperse particles, we observed bigger particles compared to the direct synthesis in the case of fast mixing conditions (for slow mixing conditions, the results were consistent with the literature). This highlights not only the importance of mass transfer, but also the effect of preconditioning the reagents on the particle formation kinetics during the Turkevich synthesis.

In the noble metal NP syntheses investigated, different synthesis conditions yielded the most monodisperse NPs. The most monodisperse silver NPs were synthesized *via* the dropwise addition of a concentrated precursor solution to the reducing agent solution, whereas the most monodisperse gold NPs were synthesized *via* the fast addition of the concentrated precursor solution to the reducing agent solution. These syntheses showed also the highest reproducibility based on the position of the surface plasmon absorption peak, making them promising reaction conditions for further studies on the reproducible synthesis of monodisperse noble metal NPs. This study highlights the importance of mixing conditions and the order of reagent addition in determining the size and polydispersity of the synthesized NPs, even when the final nominal concentrations of the reducing agent to precursor are the same. Often, batch reactor studies state only the molar ratio of the reagents used in the syntheses, but this may be insufficient information to reproduce results, since the way reagents are mixed plays a crucial role.

Conflicts of interest

There are no conflicts to declare.

Acknowledgements

The authors would like to thank EPSRC (grant EP/M015157/1 and studentship for RB). N. T. K. Thanh thanks The Royal Society for her University Research Fellowship. Furthermore, the authors thank Dr. Joseph C. Bear (Kingston University, UK) for fruitful conversations.

References

1 Z.-J. Jiang, C.-Y. Liu and L.-W. Sun, *J. Phys. Chem. B*, 2005, **109**, 1730–1735.
2 R. Mata, J. Reddy Nakkala and S. Rani Sadras, *Mater. Sci. Eng., C*, 2015, **51**, 216–225.
3 Y. Yang, S. Matsubara, L. Xiong, T. Hayakawa and M. Nogami, *J. Phys. Chem. C*, 2007, **111**, 9095–9104.
4 K. G. Stamplecoskie and J. C. Scaiano, *J. Phys. Chem. C*, 2015, **115**, 1403–1409.
5 D. Chen, X. Qiao, X. Qiu and J. Chen, *J. Mater. Sci.*, 2009, **44**, 1076–1081.
6 N. Matsuhisa, D. Inoue, P. Zalar, H. Jin, Y. Matsuba, A. Itoh, T. Yokota, D. Hashizume and T. Someya, *Nat. Mater.*, 2017, **16**, 834.
7 C. Marambio-Jones and E. M. V. Hoek, *J. Nanopart. Res.*, 2010, **12**, 1531–1551.
8 D. A. Gonzalez-Carter, B. F. Leo, P. Ruenraroengsak, S. Chen, A. E. Goode, I. G. Theodorou, K. F. Chung, R. Carzaniga, M. S. P. Shaffer, D. T. Dexter, M. P. Ryan and A. E. Porter, *Sci. Rep.*, 2017, **7**, 42871.
9 C. Mitra, P. M. Gummadidala, K. Afshinnia, R. C. Merrifield, M. Baalousha, J. R. Lead and A. Chanda, *Environ. Sci. Technol.*, 2017, **51**, 8085–8093.
10 B. Le Ouay and F. Stellacci, *Nano Today*, 2015, **10**, 339–354.
11 A. D. McFarland and R. P. Van Duyne, *Nano Lett.*, 2003, **3**, 1057–1062.
12 A. Contino, G. Maccarrone, M. Zimbone, R. Reitano, P. Musumeci, L. Calcagno and I. P. Oliveri, *J. Colloid Interface Sci.*, 2016, **462**, 216–222.
13 R. A. Sperling, P. Rivera Gil, F. Zhang, M. Zanella and W. J. Parak, *Chem. Soc. Rev.*, 2008, **37**, 1896–1908.
14 L. Dykman and N. Khlebtsov, *Chem. Soc. Rev.*, 2012, **41**, 2256–2282.
15 S. Noimark, K. Page, J. C. Bear, C. Sotelo-Vazquez, R. Quesada-Cabrera, Y. Lu, E. Allan, J. A. Darr and I. P. Parkin, *Faraday Discuss.*, 2014, **175**, 273–287.
16 G. Bodelón, C. Costas, J. Pérez-Juste, I. Pastoriza-Santos and L. M. Liz-Marzán, *Nano Today*, 2017, **13**, 40–60.
17 T. J. Macdonald, K. Wu, S. K. Sehmi, S. Noimark, W. J. Peveler, H. du Toit, N. H. Voelcker, E. Allan, A. J. MacRobert, A. Gavriilidis and I. P. Parkin, *Sci. Rep.*, 2016, **6**, 39272.
18 X. Zhang, *Cell Biochem. Biophys.*, 2015, **72**, 771–775.
19 S. Guo and E. Wang, *Anal. Chim. Acta*, 2007, **598**, 181–192.
20 B. Hafsi, A. Boubaker, D. Guerin, S. Lenfant, S. Desbief, F. Alibart, A. Kalboussi, D. Vuillaume and K. Lmimouni, *Org. Electron.*, 2017, **50**, 499–506.
21 M.-C. Daniel and D. Astruc, *Chem. Rev.*, 2004, **104**, 293–346.
22 B. S. Takale, M. Bao and Y. Yamamoto, *Org. Biomol. Chem.*, 2014, **12**, 2005–2027.
23 N. Li, P. Zhao and D. Astruc, *Angew. Chem., Int. Ed.*, 2014, **53**, 1756–1789.
24 J. Piella, N. G. Bastús and V. Puntes, *Chem. Mater.*, 2016, **28**, 1066–1075.
25 G. Caygill, M. Zanfir and A. Gavriilidis, *Org. Process Res. Dev.*, 2006, **10**, 539–552.
26 J. Bałdyga and J. R. Bourne, *Turbulent Mixing and Chemical Reactions*, Wiley, Chichester, 1999.
27 P. N. Sharratt, *Handbook of Batch Process Design*, Springer Science & Business Media, London, 1997.
28 J. Polte, R. Erler, A. F. Thünemann, S. Sokolov, T. T. Ahner, K. Rademann, F. Emmerling and R. Kraehnert, *ACS Nano*, 2010, **4**, 1076–1082.
29 J. Polte, X. Tuaev, M. Wuithschick, A. Fischer, A. F. Thuenemann, K. Rademann, R. Kraehnert and F. Emmerling, *ACS Nano*, 2012, **6**, 5791–5802.
30 D. L. Van Hyning, W. G. Klemperer and C. F. Zukoski, *Langmuir*, 2001, **17**, 3128–3135.
31 B. H. Ryu, Y. Choi, H. S. Park, J. H. Byun, K. Kong, J. O. Lee and H. Chang, *Colloids Surf., A*, 2005, **270**, 345–351.
32 V. V. Pinto, M. J. Ferreira, R. Silva, H. A. Santos, F. Silva and C. M. Pereira, *Colloids Surf., A*, 2010, **364**, 19–25.

33 N. Shirtcliffe, U. Nickel and S. Schneider, *J. Colloid Interface Sci.*, 1999, **211**, 122–129.
34 K. C. Song, S. M. Lee, T. S. Park and B. S. Lee, *Korean J. Chem. Eng.*, 2009, **26**, 153–155.
35 A. Thøgersen, J. Bonsak, C. H. Fosli and G. Muntingh, *J. Appl. Phys.*, 2011, **110**, 044306.
36 S. Agnihotri, S. Mukherji and S. Mukherji, *RSC Adv.*, 2014, **4**, 3974–3983.
37 J. Turkevich, P. C. Stevenson and J. Hillier, *Discuss. Faraday Soc.*, 1951, **11**, 55–75.
38 G. Frens, *Nat. Phys. Sci.*, 1973, **241**, 20–22.
39 S. L. Goodman, G. M. Hodges, L. K. Trejdosiewicz and D. C. Livingston, *J. Microsc.*, 1981, **123**, 201–213.
40 M. K. Chow and C. F. Zukoski, *J. Colloid Interface Sci.*, 1994, **165**, 97–109.
41 F. Kettemann, A. Birnbaum, S. Witte, M. Wuithschick, N. Pinna, R. Kraehnert, K. Rademann and J. Polte, *Chem. Mater.*, 2016, **28**, 4072–4081.
42 S. K. Sivaraman, S. Kumar and V. Santhanam, *J. Colloid Interface Sci.*, 2011, **361**, 543–547.
43 F. Schulz, T. Homolka, N. G. Bastús, V. Puntes, H. Weller and T. Vossmeyer, *Langmuir*, 2014, **30**, 10779–10784.
44 I. Ojea-Jiménez, N. G. Bastús and V. Puntes, *J. Phys. Chem. C*, 2011, **115**, 15752–15757.
45 M. Wuithschick, A. Birnbaum, S. Witte, M. Sztucki, U. Vainio, N. Pinna, K. Rademann, F. Emmerling, R. Kraehnert and J. Polte, *ACS Nano*, 2015, **9**, 7052–7071.
46 A. Henglein, *Chem. Mater.*, 1998, **10**, 444–450.
47 J. Shen, Z. Li, Q. Yan and Y. Chen, *J. Phys. Chem.*, 1993, **97**, 8504–8511.
48 J. C. Fanning, B. C. Brooks, A. B. Hoeglund, D. A. Pelletier and J. A. Wadford, *Inorg. Chim. Acta*, 2000, **310**, 115–119.
49 R. Baber, L. Mazzei, N. T. K. Thanh and A. Gavriilidis, *Nanoscale*, 2017, **9**, 14149–14161.
50 D. L. Van Hyning, W. G. Klemperer and C. F. Zukoski, *Langmuir*, 2001, **17**, 3120–3127.
51 M. Takesue, T. Tomura, M. Yamada, K. Hata, S. Kuwamoto and T. Yonezawa, *J. Am. Chem. Soc.*, 2011, **133**, 14164–14167.
52 D. L. Van Hyning and C. F. Zukoski, *Langmuir*, 1998, **14**, 7034–7046.
53 M. Wuithschick, S. Witte, F. Kettemann, K. Rademann and J. Polte, *Phys. Chem. Chem. Phys.*, 2015, **17**, 19895–19900.
54 A. P. LaGrow, T. M. D. Besong, N. M. AlYami, K. Katsiev, D. H. Anjum, A. Abdelkader, P. M. F. J. Costa, V. M. Burlakov, A. Goriely and O. M. Bakr, *Chem. Commun.*, 2017, **53**, 2495–2498.
55 K. L. Kelly, E. Coronado, L. L. Zhao and G. C. Schatz, *J. Phys. Chem. B*, 2003, **107**, 668–677.
56 J. Polte, *CrystEngComm*, 2015, **17**, 6809–6830.
57 X. Ji, X. Song, J. Li, Y. Bai, W. Yang and X. Peng, *J. Am. Chem. Soc.*, 2007, **129**, 13939–13948.
58 I. Ojea-Jiménez and J. M. Campanera, *J. Phys. Chem. C*, 2012, **116**, 23682–23691.